Demonstration of a Quantum Gate Using Electromagnetically Induced Transparency

K. McDonnell⬤, L. F. Keary, and J. D. Pritchard⬤[*]
EQOP, Department of Physics, University of Strathclyde,
SUPA, Glasgow G4 0NG, United Kingdom

We demonstrate a native CNOT gate between two individually addressed neutral atoms based on electromagnetically induced transparency. This protocol utilizes the strong long-range interactions of Rydberg states to enable conditional state transfer on the target qubit when operated in the blockade regime. An advantage of this scheme is it enables implementation of multiqubit CNOT^k gates using a pulse sequence independent of qubit number, providing a simple gate for efficient implementation of digital quantum algorithms and stabilizer measurements for quantum error correction. We achieve a loss corrected gate fidelity of $\mathcal{F}^{\text{cor}}_{\text{CNOT}} = 0.82(6)$, and prepare an entangled Bell state with $\mathcal{F}^{\text{cor}}_{\text{Bell}} = 0.66(5)$, limited at present by laser power. We present a number of technical improvements to advance this to a level required for fault-tolerant scaling.

Neutral atoms are a promising candidate for scalable quantum computing, pairing long coherence times with strong long-range interactions of highly excited Rydberg states [1–5]. Major advantages over other technologies are the ease with which the system can be scaled to create deterministically loaded, defect-free arrays of single atoms in one [6], two [7,8], and three dimensions [9,10] or through use of atomic ensembles [11]. Additionally the exquisite control over the atom-atom interactions offered through choice of Rydberg state and tuning using external static [12], microwave [13–15], or optical [16] electric fields to engineer highly anisotropic interactions with variable length scale. The strong long-range interactions give rise to a blockade mechanism whereby within a volume of radius $R \lesssim 10~\mu\text{m}$ only a single Rydberg excitation can be created [17]. Rydberg blockade can be exploited to create deterministic entanglement [18–21] or realize high-fidelity two-qubit gate operations [22–27]. These gates have enabled recent demonstration of quantum algorithms [28], with the ability to engineer nonlocal qubit connectivity through use of mobile tweezers to dynamically rearrange atoms [29].

The strong interactions can be further extended to perform native multiqubit gates [30–42] providing a route to efficient implementation of quantum circuits [43,44]. These gates can be realized using sequential excitation pulses applied to each qubit [31–34], or through simultaneous addressing [37,40] as recently demonstrated for a three qubit Toffoli gate [26]. For both approaches, pulse-shaping and quantum optimal control techniques have been utilized to obtain high-fidelity protocols [26,45,46]. However, due to the $\sqrt{N}$ scaling of the collective Rabi frequency for Rydberg excitation in the blockade regime, these protocols require reoptimization as the number of

qubits changes. An alternative approach based on electromagnetically induced transparency (EIT) was originally proposed by Müller *et al.* [42]. This scheme provides a scalable approach to performing multiqubit gates with a single control and k target qubits (CNOT^k) without the need to compensate for the collectively enhanced Rabi frequency, enabling implementation using a pulse sequence that is independent of k.

In this Letter we present the first demonstration of this EIT gate protocol for two qubits, verifying the ability to perform a native CNOT gate without requiring additional single qubit rotations, yielding a loss corrected gate fidelity of $\mathcal{F}^{\text{cor}}_{\text{CNOT}} = 0.82(6)$. We utilize this gate sequence to prepare an entangled Bell state with a corrected fidelity of $\mathcal{F}^{\text{cor}}_{\text{Bell}} = 0.66(5)$. While our current demonstration is limited by laser power, we propose a number of technical improvements to reach sufficiently high fidelities to facilitate the creation of entangled states for performing measurements beyond the standard quantum limit [47], and achieving fault-tolerant computing using surface codes for topological error correction [48].

The CNOT gate protocol proposed by Müller *et al.* [42] is illustrated in Fig. 1, with control and target atoms with states $|i\rangle_{c,t}$, respectively, where $i = 0,\ 1$ correspond to computational basis states and $i = e,\ r$ are the intermediate excited and Rydberg states respectively. We consider two atoms that are optically trapped at a separation R [Fig. 1(a)], and individually addressed. The control qubit is coupled from $|1\rangle_c \rightarrow |r\rangle_c$ by a laser with Rabi frequency Ω_r and the target qubit is addressed by a pair of ground-state Raman lasers each with Rabi-frequency $\Omega_p(t)$ driving a two-photon resonance from $|1\rangle_t \rightarrow |0\rangle_t$ with detuning Δ from the intermediate excited state $|e\rangle_t$. A strong coupling
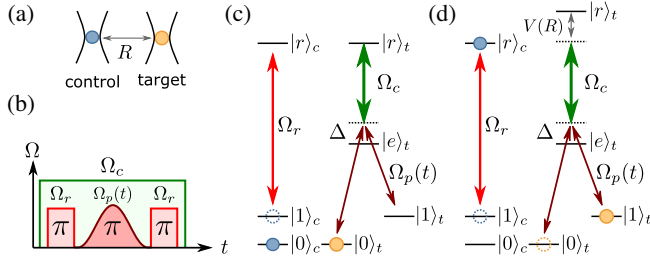
FIG. 1. EIT gate protocol. (a) A single control and target atom trapped in two optical dipole traps separated by distance R. (b) CNOT pulse sequence. (c) If the control atom is in $|0\rangle_c$ during the smooth pulse the target qubit adiabatically follows the EIT dark state $|0\rangle_t \to |0\rangle_t$ leaving its state unchanged. (d) If the control atom is initially in $|1\rangle_c$ then strong dipole-dipole interactions $V(R)$ detune the target qubit Rydberg state, breaking the EIT resonance and enabling resonant transfer $|0\rangle_t \to |1\rangle_t$.

laser with detuning $-\Delta$ couples $|e\rangle_t \to |r\rangle_t$ with Rabi frequency Ω_c. The temporal excitation sequence for the CNOT gate protocol is shown in Fig. 1(b), where a π pulse is applied to the control qubit followed by a smooth adiabatic pulse with area $A = \int dt \Omega_p(t)^2/2\Delta = \pi$ on the target qubit, then a final π pulse on the control qubit.

For the case of the control atom initially in state $|0\rangle_c$ as shown in Fig. 1(c), the Hamiltonian for the target qubit is given by

$$\mathcal{H}_t = \hbar\Omega_p(t)/2(|1\rangle_t\langle e| + |0\rangle_t\langle e|)$$
$$+ \hbar\Omega_c/2|e\rangle_t\langle r| - \hbar\Delta|e\rangle_t\langle e| + \text{H.c.}, \quad (1)$$

which for $|\Delta| \gg \Omega_p(t), \Omega_c$ allows adiabatic elimination of the intermediate $|e\rangle_t$. The resulting Hamiltonian has two EIT dark states $|d_1\rangle_t = (|1\rangle_t - |0\rangle_t)/\sqrt{2}$ and $|d_2\rangle_t = (1+x^2)^{-1/2}[(|1\rangle_t + |0\rangle_t)/\sqrt{2} - x|r\rangle_t]$ with $x = \sqrt{2}\Omega_p(t)/\Omega_c$ [42].

For $\Omega_c/\Omega_p^{\text{max}} \gtrsim 2$, and with the target qubit initially in an arbitrary state $|\psi\rangle_t = \alpha|d_1\rangle + \beta|d_2\rangle$, during the smooth Raman pulse the qubit adiabatically follows the dark state corresponding to $|0\rangle_c|\psi\rangle_t \to |0\rangle_c|\psi\rangle_t$.

If instead the control qubit is in state $|1\rangle_c$, the initial π pulse transfers population to $|r\rangle_c$ resulting in detuning of the target Rydberg state by the dipole-dipole interaction energy $V(R)$ as shown in Fig. 1(d). This modifies the target Hamiltonian to $\mathcal{H}'_t = \mathcal{H}_t + V(R)|r\rangle_t\langle r|$, which for $V(R) > \hbar\Omega_c^2/(4\Delta)$ is sufficient to break the EIT condition enabling the target qubit to undergo a Raman π pulse. This protocol thus realizes a native CNOT gate corresponding to the mapping $|1\rangle_c|0\rangle_t \leftrightarrow |1\rangle_c|1\rangle_t$.

The experiment setup, previously described in Ref. [19] and illustrated schematically in Fig. 2(a), uses a pair of individually trapped ^{133}Cs atoms separated by 6 μm that are cooled to 5 μK and detected using fluorescence collected on a sCMOS camera [49]. Qubits are encoded in the hyperfine clock states, with $|1\rangle = |6S_{1/2}, F = 4, m_F = 0\rangle$ and $|0\rangle = |6S_{1/2}, F = 3, m_F = 0\rangle$. Atoms are prepared in $|1\rangle$
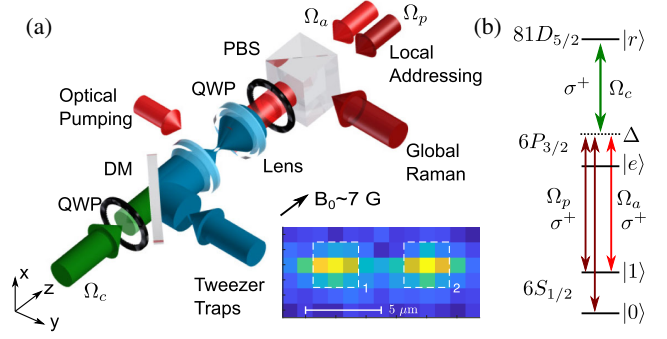

FIG. 2. Experiment setup. (a) Schematic showing single atoms trapped in microscopic tweezer traps, overlapped with the Rydberg laser on a dichroic mirror (DM) and circularly polarized using a quarter wave plate (QWP). The Raman and qubit lasers are combined on a polarizing beam splitter (PBS) and counterpropagate with the Rydberg and trapping lasers. (b) Qubit level scheme with $|1\rangle = |6S_{1/2}, F = 4, m_F = 0\rangle$, $|0\rangle = |6S_{1/2}, F = 3, m_F = 0\rangle$, and $|r\rangle = |81D_{5/2}, m_j = 5/2\rangle$. The qubit (red) and Rydberg (green) lasers drive a two-photon transition from $|1\rangle \to |r\rangle$ detuned by Δ from the intermediate state $|e\rangle$. The Raman laser Ω_p (brown) drives transitions between $|1\rangle \to |0\rangle$, and is phase locked to Ω_a.

using a linearly polarized optical pumping beam resonant with the transition from $|6S_{1/2}, F = 4\rangle \to |6P_{1/2}, F' = 4\rangle$, and we implement destructive state detection using a strong resonant blow-away beam to remove atoms in $F = 4$ prior to imaging. To overcome limitations in optical pumping fidelity due to finite polarization purity, after preparation in $|1\rangle$ we apply a resonant microwave π pulse from $|1\rangle \to |0\rangle$ followed by a blow-away pulse to eject atoms from $F = 4$ to eliminate errors from states outside the computational basis [50]. To suppress ac Stark shifts and Rydberg antitrapping from the dipole trap beam, trap light is extinguished for 5 μs during which the EIT gate pulses are applied.

For demonstration of the EIT gate protocol we utilize the laser couplings shown in Fig. 2(b). Rydberg excitation to $81D_{5/2}$ is performed using two-photon excitation via the $6P_{3/2}$ intermediate excited state. An 852 nm diode laser with Rabi frequency Ω_a couples $|1\rangle_c \to |e\rangle_c$ with detuning Δ, and a frequency doubled Ti:sapphire laser at 509 nm with detuning $\Delta_c \sim -\Delta$ and Rabi frequency Ω_c couples from $|e\rangle_c \to |r\rangle_c$. These lasers are locked to an ultralow expansion (ULE) cavity to obtain sub-kHz linewidths [53] using a detuning of $\Delta/2\pi = 870$ MHz from the $|6S_{1/2}, F = 4\rangle \to |6P_{3/2}, F' = 5\rangle$ transition. The qubit laser Ω_a is focused to a waist of 3 μm to locally address the control qubit, while the coupling laser is focused down to a $1/e^2$ waist of 18 μm to illuminate both control and target atoms equally. Both beams are σ^+ polarized to maximize coupling from $|1\rangle \to |81D_{5/2}, m_j = 5/2\rangle$ resulting in a two-photon Rabi frequency of $\Omega_r/2\pi = 1.77$ MHz.

The Raman laser driving two-photon couplings from $|1\rangle \rightarrow |0\rangle$ is derived from a second 852 nm diode laser which uses an electro-optic modulator to generate sidebands at ± 4.6 GHz before filtering out the carrier using a Mach-Zehnder interferometer [54] to obtain copropagating Raman beams with equal amplitude [19]. To ensure the Raman laser meets the EIT resonance condition, the carrier is phase-locked to the qubit laser (ω_a) to transfer the narrow linewidth while ensuring both target and control atoms have a common intermediate state detuning with the coupling laser. The Raman light is aligned onto the target qubit using a tightly focused beam waist of 3 µm with Rabi frequency $\Omega_p(t)$ and σ^+ polarization to perform local operations and EIT. A second orthogonally polarized Raman beam with a $1/e^2$ waist of 15 µm is used to perform global operations on both qubits. This beam has an additional 80 MHz detuning from the intermediate level to avoid creating additional EIT resonances with states $m_j = +1/2, 3/2$.

To implement the CNOT protocol we use an acousto-optical modulator to apply a smooth adiabatic pulse to the target qubit of the form $\Omega_p(t) = \Omega_p^{\max}(t)[1 - \cos(2\pi t/\tau)]/2$, resulting in a pulse area of $A = 3\tau\Omega_p^{\max}/8$, where τ is the pulse duration and $\Omega_p^{\max}$ is the peak two-photon Rabi frequency from $|0\rangle_t \rightarrow |1\rangle_t$. The description above presents a simplified picture as two-photon excitation via $6P_{3/2}$ involves not one but four intermediate hyperfine states $|f_e, m_f = 1\rangle_t$ coupled to the target qubit [Fig. 3(a)]. Only $f_e = 3, 4$ contribute to the Raman and EIT resonance, while the $f_e = 2$ and 5 states provide independent routes for Rydberg excitation from $|1\rangle$ or $|0\rangle$ and contribute significant ac Stark shifts to the Raman resonance. While the ac shifts evolve dynamically during the pulse sequence, we find applying a fixed detuning of the Raman laser is sufficient to obtain high fidelity state transfer. To optimize pulse parameters the smooth adiabatic Raman pulse is applied in the absence of the coupling laser and the peak power and detuning adjusted to maximize the state transfer $|1\rangle_t \rightarrow |0\rangle_t$, with results shown in Figs. 3(b) and 3(c). For a $\tau = 2$ µs pulse duration the total peak power in the Raman beam is 110 nW, corresponding to $\Omega_p^{\max}/2\pi = 0.67$ MHz and an optimal Raman detuning of $\delta/2\pi = 0.28(2)$ MHz in excellent agreement with theory [50].

Following optimization of coherent state transfer, the coupling laser is then applied and its detuning is scanned to locate the EIT resonance corresponding to the frequency at which $|1\rangle_t \rightarrow |1\rangle_t$. Data in Figs. 3(d)–3(f) show EIT scans as a function of pulse duration for $\tau = 1.5, 2$ and 3 µs, taken with a coupling power of 170 mW corresponding to a coupling Rabi frequency of $\Omega_c/2\pi \sim 40$ MHz for $f_e = 3$, 4. In each case, the data are compared to numeric simulations with good qualitative agreement with the theoretical model with additional features in the spectra coming from the hyperfine structure of the intermediate
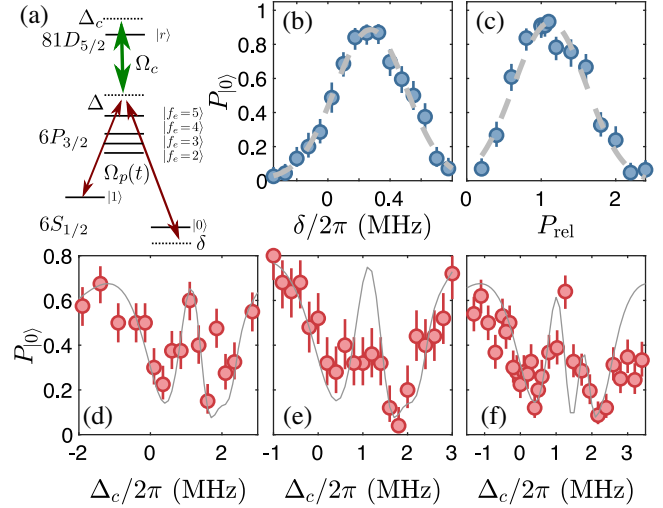

FIG. 3. Pulse optimization. (a) Target atom qubit excitation scheme, showing all the hyperfine levels of the intermediate state $6P_{3/2}$. (b) Smooth-pulse optimization with $\Omega_c = 0$ to maximize transfer $|1\rangle \rightarrow |0\rangle$ as a function of two-photon detuning δ and (c) relative pulse power P_{rel} for $\tau = 2$ µs. (d)–(f) EIT optimization vs coupling laser detuning for $\tau = 1.5, 2, 3$ µs to find EIT resonance where state transfer is suppressed due to adiabatic following of the dark state $|1\rangle \rightarrow |1\rangle$. Data are overlaid with theoretical model (gray line) [50].

$6P_{3/2}$ level [50]. For $\tau = 1.5$ µs the resulting EIT is not well defined, with leakage to $|1\rangle_t$ at all detunings due to the finite ratio $\Omega_c/\Omega_p \lesssim 1$. For longer pulse durations we observe suppression of state transfer on the EIT resonance. Below we use $\tau = 2$ µs to minimize the time the control qubit is required to remain in the Rydberg state. For this duration with $\Delta_c/2\pi = 1.8$ MHz we measure $P_{|0\rangle_t} = 0.04(10)$, showing minimal leakage during the adiabatic pulse evolution.

Using the optimized pulse parameters on the target qubit we proceed to demonstrate the CNOT gate operation applied to the two qubits, where for a 6 µm separation $V(R)/2\pi = 35$ MHz [55]. To characterize the gate operation we prepare atoms in each of the four computational basis states using microwave pulses and measure the resulting output states. Local microwave operations are implemented using the method of Xia et al. [56] by applying a calibrated ac Stark shift on the control qubit to ensure it undergoes a 4π rotation during the target qubit operation [50]. Using destructive blow away it is not possible to discriminate between atom loss events and an atom in $F = 4$ being removed from the trap. To overcome this issue, after the gate is applied we rotate each of the basis states into $|00\rangle$ to allow measurements conditioned on two-atom survivals, and the resulting corrected output probabilities are obtained by rescaling the raw two-atom survivals by the two-atom survival probability when no blow away beam is applied. We characterize our ability to prepare and measure
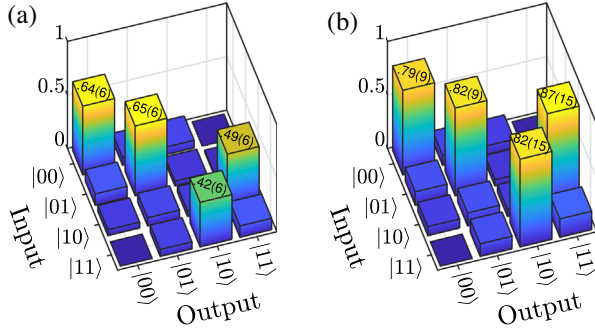
FIG. 4. Gate measurement. (a) Raw and (b) loss-corrected CNOT gate data with fidelities of $\mathcal{F}_{\mathrm{CNOT}} = 0.55(3)$ and $\mathcal{F}_{\mathrm{CNOT}}^{\mathrm{cor}} = 0.82(6)$.

computational states using this technique, resulting in raw and corrected state preparation fidelities given by $\mathcal{F}_{\mathrm{prep}} = 1/4\mathrm{Tr}(U_{\mathrm{meas}}^{T} * U_{\mathrm{ideal}}) = 0.81(2)$ and $0.91(4)$, respectively, and an average two-atom survival probability of $0.89(1)$ [50].

The EIT gate matrix is shown in Fig. 4, with the uncorrected measurements clearly revealing the characteristic structure of the native CNOT gate and verifying that for the control qubit in $|0\rangle_c$ the EIT on the target site maintains its initial state while for the control atom in $|1\rangle_c$ we obtain a rotation of the target states. From the raw data we see the probability of survival is reduced by $\sim 25\%$ when the control atom is excited to the Rydberg state due to additional losses of the control atom from the Rydberg state. This loss is dominated by the finite laser phase noise which reduces the probability of the control qubit returning to $|1\rangle_c$ after the two π pulses [26], and is much larger than the $< 5\%$ loss predicted from radiative decay and off-resonant scattering from the coupling laser during the $\tau = 2$ μs the control atom is in the Rydberg state [50]. The raw gate fidelity is $\mathcal{F}_{\mathrm{CNOT}} = 0.55(3)$, and in Fig. 4(b) we show that renormalizing the elements by the two-atom survival probability results in comparable values for all nonzero elements and a corrected gate fidelity of $\mathcal{F}_{\mathrm{CNOT}}^{\mathrm{cor}} = 0.82(6)$.

To demonstrate the CNOT protocol is able to generate deterministic entanglement we prepare atoms in the $|\Phi^+\rangle = (|00\rangle + |11\rangle)/\sqrt{2}$ Bell state using the gate sequence shown in Fig. 5(a). For these measurements state preparation is performed using the Raman lasers rather than microwaves to ensure the phase of the input state is well defined with respect to the phase of the Raman pulse applied during the gate. We apply a local $X(\pi/2)$ to the target qubit, followed by a global $X(\pi/2)$ pulse. The delay between pulses is chosen such that the target qubit accumulates phase $Z(\pi)$ to map $|00\rangle \to (|00\rangle + i|10\rangle)/\sqrt{2}$ [50] which is converted to $|\Phi^+\rangle$ following application of the CNOT gate. Bell state populations are shown in Fig. 5(b), with direct measurement of ρ_{00} (ρ_{11}) performed from measurement of two-atom survivals with (without) a
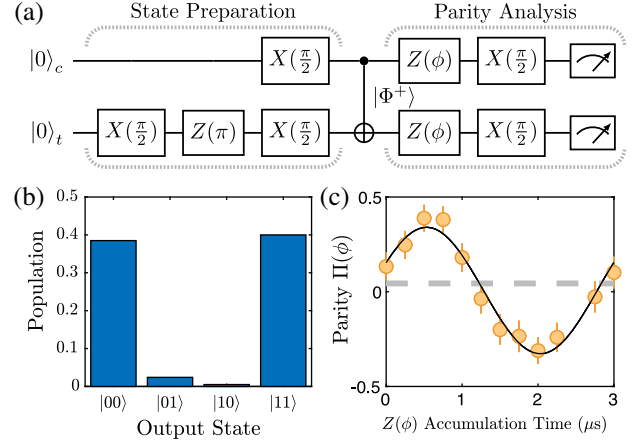

FIG. 5. Bell state preparation. (a) Gate sequence applied for Bell state preparation and analysis. (b) Measured Bell state populations. (c) Parity oscillation with amplitude $|c| = 0.17(1)$.

global $X(\pi)$ pulse applied, and the remaining elements estimated using the lower bound of [20].

The fidelity of the generated Bell state is equal to $\mathcal{F}_{\mathrm{Bell}} = \langle\Phi^+|\rho|\Phi^+\rangle = (\rho_{00} + \rho_{11})/2 + |c|$, where $c = |c|e^{i\phi_c}$ is the coherence between $|00\rangle$ and $|11\rangle$. The coherence is measured using parity oscillations after a global phase accumulation $Z(\phi)$ and global rotation $X(\pi/2)$, where phase accumulation is realized by varying the delay prior to the final analysis pulse [57]. The resulting parity $\Pi(\phi) = \rho_{00} + \rho_{11} - \rho_{01} - \rho_{10} = 2\mathrm{Re}(d) - 2|c|\cos(2\phi + \phi_c) + \rho_{xx}$, where d is the coherence between $|01\rangle$ and $|10\rangle$ and ρ_{xx} is the two-atom loss probability [50]. Figure 5(c) shows the measured parity oscillation, corresponding to a Bell state coherence with amplitude $|c| = 0.17(3)$ and an average value $\langle\Pi\rangle_\phi = 0.04(2)$ in good agreement with $\rho_{xx} = 0.06(2)$ measured independently in the absence of the state-selective blow away beam.

Combining the measurements of population and coherence, we find a raw fidelity of $\mathcal{F}_{\mathrm{Bell}} = 0.44(5)$ which lies below the threshold for entanglement and below the theoretically predicted value of 0.78 [50] due to the enhanced losses discussed above. However, from our loss-corrected population measurements, and rescaling the coherence by the average two-atom survival without blow-away $P = 0.67(5)$, we obtain a corrected fidelity of $\mathcal{F}_{\mathrm{Bell}}^{\mathrm{cor}} = 0.66(7)$, demonstrating the gate protocol is capable of generating entangled quantum states.

In conclusion, we have presented the first realization of a native CNOT gate between two neutral atoms based on EIT. Correcting for losses we obtain a gate fidelity $\mathcal{F}_{\mathrm{CNOT}}^{\mathrm{cor}} = 0.82(6)$ and demonstrate coherent parity oscillations of a $|\Phi^+\rangle$ Bell state achieving $\mathcal{F}_{\mathrm{Bell}}^{\mathrm{cor}} = 0.66(7)$. The major limitations in the current implementation arise from technical dephasing noise in the Rydberg excitation lasers which prevent high fidelity recovery of the control atom from the Rydberg state, and the limited power available for

the coupling laser which reduces the gate speed, increasing the time the control qubit must remain in the Rydberg manifold.

This limitation can be circumvented using two-photon excitation via $7P_{1/2}$, which benefits from reduced scattering and ac Stark shift errors due to having fewer intermediate hyperfine levels, a reduction in excited state linewidth $\sim \times 1/5$ and can utilize high-power laser sources at 1039 nm. We show that for modest parameters $\mathcal{F} > 0.998$ are achievable for 500 ns gate times [50]. This, combined with techniques to suppress laser phase noise [20], offers a route to high-fidelity gate implementation competitive with current controlled phase gates [25–27]. The primary advantage of the EIT protocol demonstrated here is the intrinsic scalability to many qubits, enabling implementation of an identical pulse sequence on k target qubits to realize a CNOT^k that provides an important gate for error correction [48]. Multiqubit gate fidelities are limited by residual target-target interactions, however this can be suppressed using a combination of geometric arrangement [58], careful choice of states [40] or different atomic isotopes [24] or species [59] to obtain a fidelity of $\mathcal{F}_k = 0.998^k$ [50].

The data presented in the Letter are available in Ref. [60].

Note added.—Recently, we became aware of related work calculating multiqubit gate fidelities based on this EIT protocol using heteronuclear interactions to suppress target-target couplings [61].

---

[*]jonathan.pritchard@strath.ac.uk

[1] M. Saffman, T. G. Walker, and K. Mølmer, Quantum information with Rydberg atoms, Rev. Mod. Phys. **82,** 2313 (2010).

[2] C. S. Adams, J. D. Pritchard, and J. P. Shaffer, Rydberg atom quantum technologies, J. Phys. B **53,** 012002 (2019).

[3] L. Henriet, L. Beguin, A. Signoles, T. Lahaye, A. Browaeys, G.-O. Reymond, and C. Jurczak, Quantum computing with neutral atoms, Quantum **4,** 327 (2020).

[4] M. Morgado and S. Whitlock, Quantum simulation and computing with Rydberg-interacting qubits, AVS Quantum Sci. **3,** 023501 (2021).

[5] I. Cong, H. Levine, A. Keesling, D. Bluvstein, S.-T. Wang, and M. D. Lukin, Hardware-Efficient, Fault-Tolerant Quantum Computation with Rydberg Atoms, Phys. Rev. X **12,** 021049 (2022).

[6] M. Endres, H. Bernien, A. Keesling, H. Levine, E. R. Anschuetz, A. Krajenbrink, C. Senko, V. Vuletić, M. Greiner, and M. D. Lukin, Atom-by-atom assembly of defect-free one-dimensional cold atom arrays, Science **354,** 1024 (2016).

[7] H. Kim, W. Lee, H.-g. Lee, H. Jo, Y. Song, and J. Ahn, In situ single-atom array synthesis using dynamic holographic optical tweezers, Nat. Commun. **7,** 13317 (2016).

[8] D. Barredo, S. de Léséleuc, V. Lienhard, T. Lahaye, and A. Browaeys, An atom-by-atom assembler of defect-free arbitrary two-dimensional atomic arrays, Science **354,** 1021 (2016).

[9] W. Lee, H. Kim, and J. Ahn, Three-dimensional rearrangement of single atoms using actively controlled optical microtraps, Opt. Express **24,** 9816 (2016).

[10] D. Barredo, V. Lienhard, S. de Léséleuc, T. Lahaye, and A. Browaeys, Synthetic three-dimensional atomic structures assembled atom by atom, Nature (London) **561,** 79 (2018).

[11] M. Ebert, M. Kwon, T. G. Walker, and M. Saffman, Coherence and Rydberg Blockade of Atomic Ensemble Qubits, Phys. Rev. Lett. **115,** 093601 (2015).

[12] S. Ravets, H. Labuhn, D. Barredo, T. Lahaye, and A. Browaeys, Measurement of the angular dependence of the dipole-dipole interaction between two individual Rydberg atoms at a Förster resonance, Phys. Rev. A **92,** 020701 (R) (2015).

[13] M. Tanasittikosol, J. D. Pritchard, D. Maxwell, A. Gauguet, K. J. Weatherill, R. M. Potvliege, and C. S. Adams, Microwave dressing of Rydberg dark states, J. Phys. B **44,** 184020 (2011).

[14] D. Maxwell, D. J. Szwer, D. Paredes-Barato, H. Busche, J. D. Pritchard, A. Gauguet, K. J. Weatherill, M. P. A. Jones, and C. S. Adams, Storage and Control of Optical Photons Using Rydberg Polaritons, Phys. Rev. Lett. **110,** 103001 (2013).

[15] S. Sevinçli and T. Pohl, Microwave control of Rydberg atom interactions, J. Phys. B **16,** 123036 (2014).

[16] S. de Léséleuc, D. Barredo, V. Lienhard, A. Browaeys, and T. Lahaye, Optical Control of the Resonant Dipole-Dipole Interaction between Rydberg Atoms, Phys. Rev. Lett. **119,** 053202 (2017).

[17] M. D. Lukin, M. Fleischhauer, R. Cote, L. M. Duan, D. Jaksch, J. I. Cirac, and P. Zoller, Dipole Blockade and Quantum Information Processing in Mesoscopic Atomic Ensembles, Phys. Rev. Lett. **87,** 037901 (2001).

[18] T. Wilk, A. Gaëtan, C. Evellin, J. Wolters, Y. Miroshnychenko, P. Grangier, and A. Browaeys, Entanglement of Two Individual Neutral Atoms Using Rydberg Blockade, Phys. Rev. Lett. **104,** 010502 (2010).

[19] C. J. Picken, R. Legaie, K. McDonnell, and J. D. Pritchard, Entanglement of neutral-atom qubits with long ground-Rydberg coherence times, Quantum Sci. Technol. **4,** 015011 (2018).

[20] H. Levine, A. Keesling, A. Omran, H. Bernien, S. Schwartz, A. S. Zibrov, M. Endres, M. Greiner, V. Vuletić, and M. D. Lukin, High-Fidelity Control and Entanglement of Rydberg-Atom Qubits, Phys. Rev. Lett. **121,** 123603 (2018).

[21] I. S. Madjarov, J. P. Covey, A. L. Shaw, J. Choi, A. Kale, A. Cooper, H. Pichler, V. Schkolnik, J. R. Williams, and M. Endres, High-fidelity entanglement and detection of alkaline-earth Rydberg atoms, Nat. Phys. 16, 857 (2020).

[22] L. Isenhower, E. Urban, X. L. Zhang, A. T. Gill, T. Henage, T. A. Johnson, T. G. Walker, and M. Saffman, Demonstration of a Neutral Atom Controlled-NOT Quantum Gate, Phys. Rev. Lett. 104, 010503 (2010).

[23] K. M. Maller, M. T. Lichtman, T. Xia, Y. Sun, M. J. Piotrowicz, A. W. Carr, L. Isenhower, and M. Saffman, Rydberg-blockade controlled-not gate and entanglement in a two-dimensional array of neutral-atom qubits, Phys. Rev. A 92, 022336 (2015).

[24] Y. Zeng, P. Xu, X. He, Y. Liu, M. Liu, J. Wang, D. J. Papoular, G. V. Shlyapnikov, and M. Zhan, Entangling Two Individual Atoms of Different Isotopes via Rydberg Blockade, Phys. Rev. Lett. 119, 160502 (2017).

[25] T. M. Graham, M. Kwon, B. Grinkemeyer, Z. Marra, X. Jiang, M. T. Lichtman, Y. Sun, M. Ebert, and M. Saffman, Rydberg Mediated Entanglement in a Two-Dimensional Neutral Atom Qubit Array, Phys. Rev. Lett. 123, 230501 (2019).

[26] H. Levine, A. Keesling, G. Semeghini, A. Omran, T. T. Wang, S. Ebadi, H. Bernien, M. Greiner, V. Vuletić, H. Pichler, and M. D. Lukin, Parallel Implementation of High-Fidelity Multiqubit Gates with Neutral Atoms, Phys. Rev. Lett. 123, 170503 (2019).

[27] Z. Fu, P. Xu, Y. Sun, Y. Y. Liu, X. D. He, X. Li, M. Liu, R. B. Li, J. Wang, L. Liu, and M. S. Zhan, High fidelity entanglement of neutral atoms via a Rydberg-mediated single-modulated-pulse controlled-PHASE gate, Phys. Rev. A 105, 042430 (2022).

[28] T. M. Graham et al., Demonstration of multi-qubit entanglement and algorithms on a programmable neutral atom quantum computer, Nature (London) 604, 457 (2022).

[29] D. Bluvstein, H. Levine, G. Semeghini, T. T. Wang, S. Ebadi, M. Kalinowski, A. Keesling, N. Maskara, H. Pichler, M. Greiner, V. Vuletić, and M. D. Lukin, A quantum processor based on coherent transport of entangled atom arrays, Nature (London) 604, 451 (2022).

[30] E. Brion, A. S. Mouritzen, and K. Mølmer, Conditional dynamics induced by new configurations for Rydberg dipole-dipole interactions, Phys. Rev. A 76, 022334 (2007).

[31] L. Isenhower, M. Saffman, and K. Mølmer, Multibit C_k-NOT quantum gates via Rydberg blockade, Quantum Inf. Process. 10, 755 (2011).

[32] I. I. Beterov, I. N. Ashkarin, E. A. Yakshina, D. B. Tretyakov, V. M. Entin, I. I. Ryabtsev, P. Cheinet, P. Pillet, and M. Saffman, Fast three-qubit Toffoli quantum gate based on three-body Förster resonances in Rydberg atoms, Phys. Rev. A 98, 042704 (2018).

[33] X.-F. Shi, Deutsch, Toffoli, and CNOT Gates via Rydberg Blockade of Neutral Atoms, Phys. Rev. Appl. 9, 051001(R) (2018).

[34] M. Li, F.-Q. Guo, Z. Jin, L.-L. Yan, E.-J. Liang, and S.-L. Su, Multiple-qubit controlled unitary quantum gate for Rydberg atoms using shortcut to adiabaticity and optimized geometric quantum operations, Phys. Rev. A 103, 062607 (2021).

[35] S.-L. Su, Y. Gao, E. Liang, and S. Zhang, Fast Rydberg antiblockade regime and its applications in quantum logic gates, Phys. Rev. A 95, 022319 (2017).

[36] J. T. Young, P. Bienias, R. Belyansky, A. M. Kaufman, and A. V. Gorshkov, Asymmetric Blockade and Multiqubit Gates via Dipole-Dipole Interactions, Phys. Rev. Lett. 127, 120501 (2021).

[37] H. Wu, R. E. George, J. H. Wesenberg, K. Mølmer, D. I. Schuster, R. J. Schoelkopf, K. M. Itoh, A. Ardavan, J. J. L. Morton, and G. A. D. Briggs, Storage of Multiple Coherent Microwave Excitations in an Electron Spin Ensemble, Phys. Rev. Lett. 105, 140503 (2010).

[38] H.-Z. Wu, Z.-B. Yang, and S.-B. Zheng, Implementation of a multiqubit quantum phase gate in a neutral atomic ensemble via the asymmetric Rydberg blockade, Phys. Rev. A 82, 034307 (2010).

[39] S. L. Su, H. Z. Shen, E. Liang, and S. Zhang, One-step construction of the multiple-qubit Rydberg controlled-phase gate, Phys. Rev. A 98, 032306 (2018).

[40] M. Khazali and K. Mølmer, Fast Multiqubit Gates by Adiabatic Evolution in Interacting Excited-State Manifolds of Rydberg Atoms and Superconducting Circuits, Phys. Rev. X 10, 021054 (2020).

[41] S. E. Rasmussen, K. Groenland, R. Gerritsma, K. Schoutens, and N. T. Zinner, Single-step implementation of high-fidelity n-bit Toffoli gates, Phys. Rev. A 101, 022308 (2020).

[42] M. Müller, I. Lesanovsky, H. Weimer, H. P. Büchler, and P. Zoller, Mesoscopic Rydberg Gate Based on Electromagnetically Induced Transparency, Phys. Rev. Lett. 102, 170502 (2009).

[43] K. Mølmer, L. Isenhower, and M. Saffman, Efficient Grover search with Rydberg blockade, J. Phys. B 44, 184016 (2011).

[44] D. Petrosyan, M. Saffman, and K. Mølmer, Grover search algorithm with Rydberg-blockaded atoms: Quantum Monte Carlo simulations, J. Phys. B 49, 094004 (2016).

[45] G. Pelegrí, A. J. Daley, and J. D. Pritchard, High-fidelity multiqubit Rydberg gates via two-photon adiabatic rapid passage, Quantum Sci. Technol. 7, 045020 (2022).

[46] S. Jandura and G. Pupillo, Time-optimal two- and three-qubit gates for Rydberg atoms, Quantum 6, 712 (2022).

[47] C. MacCormick, S. Bergamini, C. Mansell, H. Cable, and K. Modi, Supraclassical measurement using single-atom control of an atomic ensemble, Phys. Rev. A 93, 023805 (2016).

[48] J. M. Auger, S. Bergamini, and D. E. Browne, Blueprint for fault-tolerant quantum computation with Rydberg atoms, Phys. Rev. A 96, 052320 (2017).

[49] C. J. Picken, R. Legaie, and J. D. Pritchard, Single atom imaging with an sCMOS camera, Appl. Phys. Lett. 111, 164102 (2017).

[50] See Supplemental Material at http://link.aps.org/supplemental/10.1103/PhysRevLett.129.200501 for details of numerical modelling and multi-qubit gate performance alongside experimental details relating to state preparation and readout, which includes Refs. [51,52].

[51] I. I. Beterov, I. I. Ryabtsev, D. B. Tretyakov, and V. M. Entin, Quasiclassical calculations of blackbody-radiation-induced depopulation rates and effective lifetimes of Rydberg nS, nP, and nD alkali-metal atoms with n ≤ 80, Phys. Rev. A 79, 052504 (2009).

[52] A. Gaëtan, C. Evellin, J. Wolters, P. Grangier, T. Wilk, and A. Browaeys, Analysis of the entanglement between two individual atoms using global Raman rotations, New J. Phys. **12**, 065040 (2010).

[53] R. Legaie, C. J. Picken, and J. D. Pritchard, Sub-kHz excitation lasers for quantum information processing with Rydberg atoms, J. Opt. Soc. Am. B **35**, 892 (2018).

[54] M. D. D. Haubrich and R. Wynands, Lossless beam combiners for nearly equal laser frequencies, Rev. Sci. Instrum. **71**, 338 (2000).

[55] N. Šibalić, J. D. Pritchard, C. S. Adams, and K. J. Weatherill, ARC: An open-source library for calculating properties of alkali Rydberg atoms, Comput. Phys. Commun. **220**, 319 (2017).

[56] T. Xia, M. Lichtman, K. Maller, A. W. Carr, M. J. Piotrowicz, L. Isenhower, and M. Saffman, Randomized Benchmarking of Single-Qubit Gates in a 2D Array of Neutral-Atom Qubits, Phys. Rev. Lett. **114**, 100503 (2015).

[57] C. A. Sackett, D. Kielpinski, B. E. King, C. Langer, V. Meyer, C. J. Myatt, M. Rowe, Q. A. Turchette, W. M. Itano, D. J. Wineland, and C. Monroe, Experimental entanglement of four particles, Nature (London) **404**, 256 (2000).

[58] S. de Léséleuc, V. Lienhard, P. Scholl, D. Barredo, S. Weber, N. Lang, H. Buchler, T. Lahaye, and A. Browaeys, Experimental realization of a symmetry protected topological phase of interacting bosons with Rydberg atoms, Science **365**, 775 (2019).

[59] I. I. Beterov and M. Saffman, Rydberg blockade, Förster resonances, and quantum state measurements with different atomic species, Phys. Rev. A **92**, 042710 (2015).

[60] Data available from 10.15129/b883894e-434b-45ea-9b99-8db97081fea7.

[61] A. M. Farouk, I. I. Beterov, P. Xu, S. Bergamini, and I. I. Ryabtsev, Parallel implementation of $CNOT^N$ and $C_k NOT^N$ gates via homonuclear and heteronuclear Förster interactions of Rydberg atoms, arXiv:2206.12176.